J. Sens. Sens. Syst., 14, 55–65, 2025
https://doi.org/10.5194/jsss-14-55-2025


JSSS Journal of Sensors and Sensor Systems Open Access

# Investigation of the gas-sensing performance of CuO sensors functionalized with different stabilized Au nanoparticles

**Christian Maier[1], Larissa Egger[1], Anton Köck[1], Sören Becker[2], Jan Steffen Niehaus[2], and Klaus Reichmann[3]**

[1]Materials Center Leoben Forschung GmbH, Roseggerstraße 12, 8700 Leoben, Austria
[2]Fraunhofer Center for Applied Nanotechnology CAN, Grindelallee 117, 20146 Hamburg, Germany
[3]Institute for Chemistry and Technology of Materials, TU Graz, Stremayrgasse 9, 8010 Graz, Austria

**Correspondence:** Christian Maier (christian.maier@mcl.at)

Received: 27 November 2024 – Revised: 23 January 2025 – Accepted: 27 January 2025 – Published: 27 March 2025

**Abstract.** In this work, which was presented at the Eurosensors 2024 conference (Maier et al., 2024a), we present the development of chemoresistive nanosensors based on ultrathin CuO/$Cu_2O$ films, fabricated through a two-step process involving thermal evaporation and subsequent oxidation on $Si_3N_4$-based micro-hotplate chips. The semiconducting metal oxide (SMOX) gas sensors are tested against various target gases like carbon monoxide (CO), carbon dioxide ($CO_2$), and a mixture of hydrocarbons ($HC_{Mix}$). The CuO/$Cu_2O$ films are functionalized with sodium citrate and also with synthesized Au nanoparticles (Au NPs), which are stabilized with different types of ligands, namely, $\alpha$-methoxypoly(ethylene glycol)-$\omega$-(11-mercaptoundecanoate) (PEG–MUA), 3-mercaptopropionic acid (MPA), and citrate. While the Au NPs clearly increase the sensor response, in particular for $CO_2$ and $HC_{Mix}$, we have figured out that the ligands have a significant impact on the sensor performance. In order to gain further insight into the influence of the different ligands on the sensing performance, the surface was characterized by scanning electron microscopy (SEM), and the composition was determined by grazing incidence X-ray diffraction (GIXRD) measurement.

## 1 Introduction

Indoor and outdoor air quality (AQ) monitoring has become increasingly important over the last century because of the scientific advances in health aspects and regulations from the governments. Pollutant gases that are harmful or even toxic, such as CO or various volatile organic compounds (VOCs), have the potential to significantly affect human health. Additionally, elevated indoor concentrations of $CO_2$ can contribute to health issues, such as respiratory and circulatory problems or simply headaches. Metal oxides, including $SnO_2$, ZnO, and CuO, are emerging as promising candidates for gas sensing due to their sensitivity to a wide range of gases (Nikolic et al., 2020). These materials play an important role of miniaturization of gas sensors and also enable cost-effective mass production. The sensing mechanism is based on a reaction of the metal oxide and the target gas, which can be measured as a change in the electrical resistance. In recent years, there has been a massive increase in research into CuO in particular due to its low cost and high sensitivity to different gases (Rydosz, 2018). A variety of deposition technologies can be employed to fabricate CuO with different structural modifications, the investigation of which is ongoing, with some remaining issues (Maier et al., 2024b). To increase the sensor performance, CuO can be functionalized with different nanoparticles (Steinhauer, 2021), such as Au, Ru, Pd, or Pt, to reduce the operating temperature and increase the sensor response. Korotcenkov et al. (2016) summarize the effects of Au nanoparticles (NPs) on different substrates, such as $SnO_2$, $WO_3$, or ZnO, that increase the sensor response to many gases. The doping of nanoparticles enables two distinct sensing mechanisms, namely, chemical and electronic sensitization (Degler et al., 2019). In the context of chemical sensitization, the nanoparticles facilitate the

activation of gas molecules, causing a change in the concentration of adsorbed oxygen molecules on the metal oxide due to the spillover effect. In contrast, in electronic sensitization, adsorbed oxygen on the nanoparticles undergoes a transformation, leading to a direct exchange of electrons between the nanoparticles and the metal oxide (Velmathi et al., 2016). However, the investigation of material combinations involving CuO for the detection of $CO_2$ gas represents a significant area of focus in the literature as evidenced by the summary presented in reference (Maier et al., 2024c). There are many techniques, such as laser ablation, sputtering, and spray pyrolysis. to deposit the nanoparticles on the surface of the target material (Jamkhande et al., 2019). One simple and cost-effective method is drop coating. A drop of a mixture containing a solvent and the nanoparticles is deposited on the substrate (Kaliyaraj Selva Kumar et al., 2020). During the drying step, the solvent evaporates, leaving the nanoparticles on the surface. As reported in Wimmer-Teubenbacher et al. (2018), a functionalization of CuO thin films with Au NPs with a concentration of 0.0000508 mol $m^{-3}$ by drop coating can lead to a sensor response of 365 % towards 2000 ppm $CO_2$, which is 13 times higher compared to the unfunctionalized CuO film. Au NPs have to be stabilized with ligands in order to avoid an agglomeration in the solution. Typical stabilizing agents for the synthesis of Au NPs are citrate, thiolated molecules, or polyethylene glycol (PEG), which can be easily connected by ligand exchange reactions (Thambiliyagodage, 2022). In the electrodeposition of copper on silicon wafers, PEG is frequently employed as an additive with the objective of enhancing the deposition rate in cavities while simultaneously reducing the deposition rate on the surface. (Mroczka and Słodkowska, 2020). Conversely, the interaction of copper with thiolated compounds, such as 3-mercaptopropionic acid (MPA), results in the oxidation of the metal and the reduction in the thiol, which ultimately leads to the formation of a disulfide compound (Su et al., 2010). Therefore, investigations are necessary to study the effect of different ligands on the sensor performance. To our best knowledge, there are no reports of the influence of different ligands on the sensor performance, especially on the sensor response. Therefore, investigations are necessary to achieve more efficient gas sensors with reduced size, power consumption and low production cost. In this work, we fabricate three different stabilized Au NP solutions and investigate the influence of the behaviour of CuO sensors on different test gases and also the influence of humidity.

## 2 Sensor fabrication

The gas-sensitive thin films are structured with photolithography (Mask-Aligner MJB4, Süss MicroTec, Garching, Germany) on a micro-hotplate chip. The chosen sensing geometry is a circle with a diameter of 450 µm. A Cu layer with a thickness of $500 \pm 5$ nm is deposited by thermal evaporation method (UNIVEX 450, Leybold GmbH, Cologne, Germany). A deposition rate of $0.5 \pm 0.1$ nm $s^{-1}$ for Cu at $5.1 \times 10^{-6}$ mbar was used. The chip is then oxidized on a PZ28-3T hotplate (HP, Harry Gestigkeit GmbH, Düsseldorf, Germany) at $450 \pm 5$ °C for 4 h, leading to a mixture of CuO and $Cu_2O$. The temperature of the hotplate was checked using a thermocouple. The samples were heated up from room temperature in 20 min. The cooling down lasted for about 3 h. Afterwards, the samples were taken off the HP. The oxidation process parameters were chosen according to the work of de Los Santos Valladares et al. (2012)

## 3 Synthesis of Au nanoparticles

The colloidal gold nanoparticles (Au NPs) (Fig. 1a) with a diameter of $13.2 \pm 1.8$ nm used for the functionalization of the metal oxide gas sensors were synthesized by a protocol based on the work of Schulz et al. (2014) using an inverse Turkevich method. In this wet chemical approach, a citrate buffer, one part citric acid and three parts sodium citrate (Fig. 1b), was used to control the pH.

All the used glass wear was cleaned with aqua regia prior to the synthesis. In a flask, 1000 mL of the 2.5 mol $m^{-3}$ citrate buffer solution was heated to its boiling point. The solution was stirred for 10 min at this temperature. Parallel 100 mL of 2.5 mol $m^{-3}$ tetrachloroauric acid solution were heated to 85 °C and stirred at this temperature. After 10 min, this solution was quickly transferred into the boiling buffer solution. The reaction mixture was cooled to 70 °C and transferred into an appropriate container for storing.

Before the functionalization of the semiconducting metal oxide (SMOX) gas sensors, the Au NPs were isolated via centrifugation from the reaction mixture and redispersed in high-purity water. To exchange the ligands on the surface of the Au NPs, 200 µL of a 2 mol $m^{-3}$ of a 3-mercaptopropionic acid (MPA) (Fig. 1c) or $\alpha$-methoxypoly(ethylene glycol)-$\omega$-(11-mercaptoundecanoate) (PEG–MUA) (Fig. 1d) solution was added to 10 mL of the unpurified reaction mixture. The modified Au NPs were isolated via centrifugation and redispersed in high-purity water or, in the case of MPA, in a NaOH solution (pH $\sim$ 9).

## 4 Sensor functionalization and finalized device

A drop of around 0.2 µL of the citrate or Au NP solution is placed on the sensitive layer and then dried for 10 min in air. The drop coating is repeated two times to get enough Au NPs on the surface. The final sensor is illustrated in Fig. 2a.

The gas sensor device (Fig. 2b) is based on a microelectromechanical systems (MEMS)-technology-fabricated $2 \times 2$ mm $Si_3N_4$ platform chip, where the $Si_3N_4$ membrane (thickness of 900 nm, $1.02 \times 1.02$ mm) is underetched. As illustrated in Fig. 2a, the sensor consists of a heater structure (Mo) and sensor contacts (Pt with a Ti adhesion layer). The

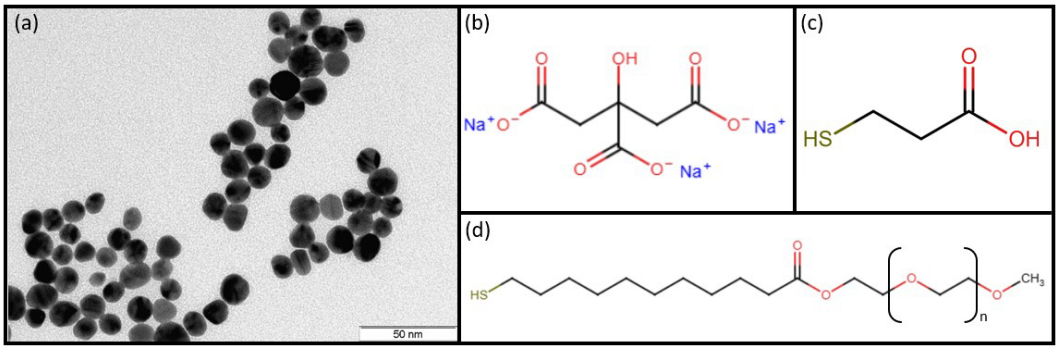


**Figure 1.** **(a)** TEM image of Au NPs stabilized with PEG–MUA, **(b)** chemical structure of ligands – sodium citrate, **(c)** 3-mercaptopropionic acid (MPA), and **(d)** $\alpha$-methoxypoly(ethylene glycol)-$\omega$-(11-mercaptoundecanoate) (PEG–MUA).

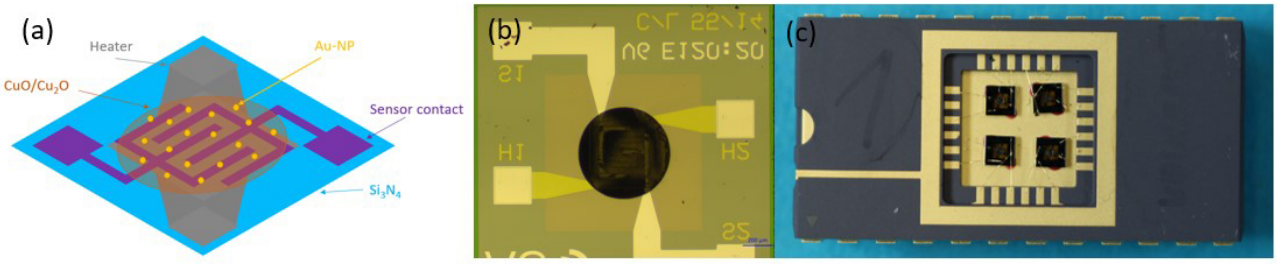


**Figure 2.** **(a)** Illustration of a functionalized $CuO/Cu_2O$ gas sensor and **(b)** images of the finalized sensor and **(c)** connection for resistance measurements.

sensor chip is then adhered by an electrically non-conductive adhesive (LOCTITE ABLESTIK 2035SC, Henkel AG & Co., Düsseldorf, Germany) to a KD-S78382-H CERAMIC DUAL INLINE PACKAGE (Kyocera Corporation, Kyoto, Japan) (Fig. 2c). Subsequently, the sensor is connected by Au wires to the ceramic platform. The finished assembly is then stacked on a printed circuit board, at which point it is ready for the measurement process in a specific self-made gas measurement box designed for constant current measurements.

## 5 Sensor characterization

Grazing incidence X-ray diffraction (GIXRD; XRDynamic 500, Anton Paar, Graz, Austria) was used to determine the present phases in the thermally oxidized sensing films used in this study. In a further study, the distribution of the Au NPs on the sensing films were characterized by SEM (Raith eLINE+, Raith GmbH, Dortmund, Germany). A self-made gas measurement setup was used to characterize the sensing performance. The determination of the resistance is done with a self-made gas measurement box by measuring the voltage while using a constant current of 1 µA. The sensor devices are tested against CO, $CO_2$, and $HC_{Mix}$ (equal mixture of 500 ppm of acetylene, ethane, ethene and propene). As the background gas, synthetic air (Linde Gas GmbH) was used, with a composition of 80 % nitrogen and 20 % oxygen. A constant flow of 1000 sccm (equals $1.67 \times 10^{-5}\,m^3\,s^{-1}$) was set by a mass flow controller (EL-FLOW, Bronkhorst High-Tech BV, Ruurlo, Netherlands). A pre-test showed that the ideal operating temperature is 300 °C. Therefore, the sensor was heated up to 300 °C. The relative humidity (RH) was varied between 25 %, 50 %, and 75 % and controlled by a commercial humidity sensor (AFK-E, KOBOLD Holding GmbH, Vienna, Austria). The influence of the different stabilized Au NPs on the response to $CO_2$ and to the other target gases was tested. Following a 5-month period, temperature dependence was taken, with the operating temperature increasing from 320 to 400 °C in 20 °C increments to gain information about sensor stability. The RH was also maintained at 50 % with 4000 ppm $CO_2$ pulses for each temperature. The sensor response was calculated with Eq. (1), where $R_g$ is the resistance during the gas exposure and $R_a$ is the resistance in synthetic air interpolated before and after the gas pulse, to compensate the possible drift of the sensor resistance.

$$S = \frac{R_g - R_a}{R_a} \cdot 100\,\% \tag{1}$$

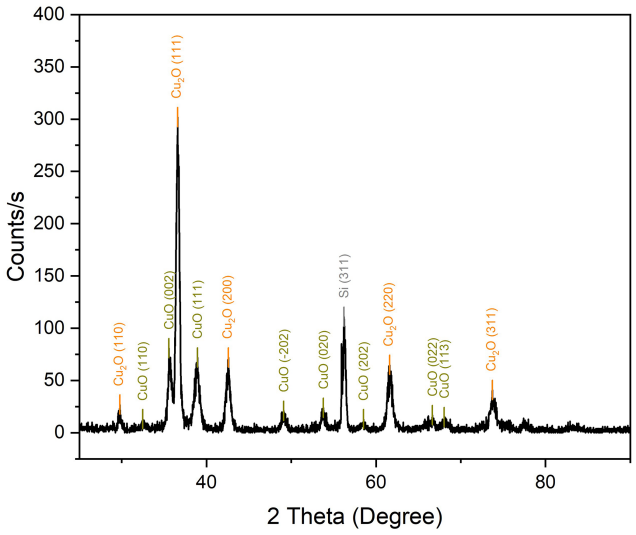


**Figure 3.** GIXRD measurement of the sensitive layer.

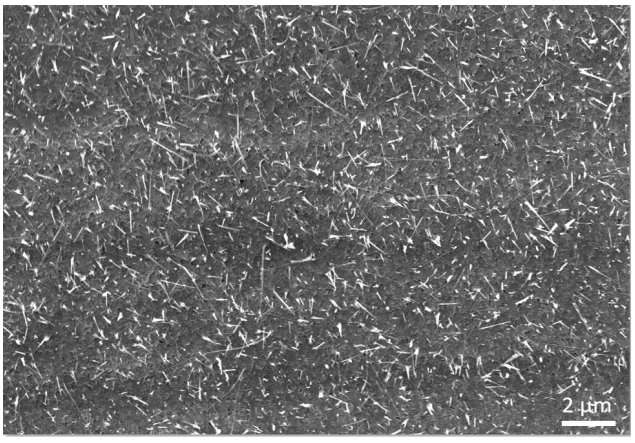


**Figure 4.** SEM picture of the sensor surface before the functionalization.

## 6 Results

### 6.1 GIXRD measurement

Figure 3 illustrates the GIXRD measurement, which was employed to gather data regarding the film composition. One of the key benefits of this technique is its capacity to precisely control the depth of penetration, which can be adjusted to a mere few nanometres (Yang et al., 2020). In the literature (Kaur et al., 2022), it is described that the oxidation of Cu to $Cu_2O$ and CuO results in the appearance of characteristic reflections. It can be observed that $Cu_2O$ (illustrated in orange) exhibits the most intense XRD $2\theta$ reflection at 36.7°, whereas CuO (illustrated in green) displays the most pronounced $2\theta$ reflections at 35.6 and 38.9°. It would appear that pure Cu displays the highest $2\theta$ reflection at 43.4°. It is shown that all of the present copper is oxidized to a mixture of CuO and $Cu_2O$ as no metallic copper is detected. In comparison to the literature (Xiong et al., 2014), it can be observed that the crystallinity is somewhat lower, as indicated by a slight broadening of the reflections. The reflection height provides information about the preferred crystal orientation marked in the round brackets at each reflection in Fig. 2. It is worth noting that a reflection of the underlying Si substrate (illustrated in grey) is detected in the sample (Tehrani, 2015).

### 6.2 SEM investigations

Figure 4 shows the sensor surface before the functionalization, where it is visible that the entire surface is covered by CuO nanowires (NWs). The NW (Mohamed and Al-Mokhtar, 2018) growth commences with the formation of a $Cu_2O$ layer on the Cu metal. Subsequent oxidation results in the formation of a CuO layer on top. Diffusion of Cu through this layer system occurs along the grain boundaries, reaching the surface where NW growth initiates. Upon attaining a specific length, the NWs fracture and deposit on the surface.

Figure 5 illustrates SEM images of the of the bare $CuO/Cu_2O$ sensing film (a) and the three functionalized films, where the ligands were different (b–d). Figure 5a shows the typical CuO NWs on a copper surface following oxidation. Figure 5b illustrates the $CuO/Cu_2O$ with the citrate-stabilized Au NPs, which tend to form large agglomerates (up to 800 nm in diameter) at an operating temperature of 300 °C. In contrast, MPA-stabilized Au NPs, illustrated with the blue circles in Fig. 5c, also form agglomerates; however, they do not undergo a coalescence process at the operation temperature of 300 °C. The presence of large PEG–MUA ligands (Fig. 5d) results in the dispersion of Au NPs across the entire surface, preventing agglomeration and melting. In comparison, the PEG–MUA ligands are of a larger size than the MPA ligands, which results in a higher stability (Schulz et al., 2013). Consequently, the Au NPs are separated on the surface by the PEG–MUA ligands. At temperatures above 300 °C, the Au NPs undergo a shape change and coalescence process, which reduces their surface energy (Wang et al., 2010). The citrate-stabilized Au NPs exhibit the highest degree of coalescence, indicating the most significant reduction in surface energy compared to the other stabilized Au NPs. Therefore, the PEG–MUA ligands that remain separated possess the highest surface energy.

### 6.3 Gas measurement

Figure 6 shows a typical gas measurement for $CO_2$, the operation temperature is 300 °C, and the relative humidity is 50 %. The resistance of the bare $CuO/Cu_2O$ film is low compared to the functionalized films. Since the bare $CuO/Cu_2O$ sensing films (red line) show no response towards $CO_2$, a special focus was set on the functionalization with the nanoparticles with the different ligands. The greatest change in resistance during $CO_2$ exposure was observed

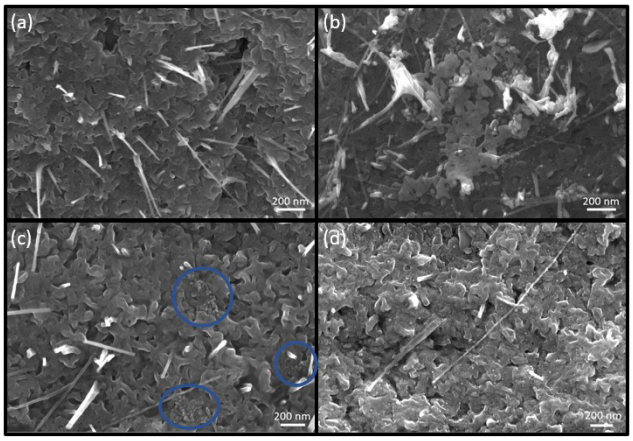


**Figure 5.** SEM picture of different stabilized Au NPs: **(a)** sensor without Au NPs, **(b)** sensor with citrate-stabilized Au NPs, **(c)** sensor with MPA-stabilized Au NPs in blue circles, and **(d)** sensor with PEG–MUA-stabilized Au NPs.

in the $CuO/Cu_2O$ layer functionalized with citrate-stabilized Au NPs (green line), followed by the citrate without Au NPs (orange line). A small change in the resistance was achieved with the MPA-stabilized (black line) Au NPs. The $CuO/Cu_2O$ functionalized with PEG–MUA Au NPs (blue line) showed the lowest or no change towards a $CO_2$ exposure. For all samples, the resistance change against 1000 and 2000 ppm is similar but increases again for 4000 ppm.

A summary of the responses calculated with Eq. 1 of each test sensing film towards CO (20 ppm), $CO_2$ (4000 ppm), and $HC_{Mix}$ (20 ppm) is shown in Fig. 7. The bare $CuO/Cu_2O$ only react to $HC_{Mix}$ with a sensor response of 4.6 % at a relative humidity level of 50 %. All of the functionalized sensors show an improvement of the sensitivity towards 20 ppm $HC_{Mix}$. Here, the PEG–MUA Au NPs had the highest sensor response of 21 %, whereas MPA Au NPs (18 %) and citrate Au NPs (17 %) are similar. The citrate without Au NPs shows a small sensor response increase to 8 %. Furthermore, it is indicated that the increase in sensor response towards $HC_{Mix}$ is not influenced by the ligand but is instead strongly influenced by the Au NPs. In the case of CO, the functionalized sensors react to the test gas, except the ones stabilized with MPA Au NPs. The highest sensor response of 9 % was reached by the citrate. The sensor response of the other functionalized sensors is smaller than 5 % towards CO. All functionalized sensors showed a sensor response to 4000 ppm of $CO_2$. The highest sensor response (39 %) was obtained for the citrate Au NPs, followed by the citrate with 26 %. The MPA Au NPs also show a significant sensor response of 10 % towards $CO_2$. The PEG–MUA Au NPs reached a sensor response of around 2 %.

Regarding to the selectivity, these results show a high potential for realizing a gas sensors array, containing the bare $CuO/Cu_2O$, the MPA Au NPs, and the citrate Au NPs. For example, if all sensors react to a gas mixture, it is a strong indicator that a $HC_{Mix}$ component is present. If both Au NP functionalized sensors react, $CO_2$ is measured. However, if only the citrate Au NPs sensor reacts, it is an indicator of CO.

### 6.4 Influence of the relative humidity

The relative humidity (RH) has been shown to have a significant impact on the resistance baseline of SMOX-based sensors (see Fig. 8, which illustrates the resistance change normalized to 25 % RH). The used normalized resistance change is calculated after Eq. (2), where $R_{x\,\mathrm{RH}}$ is the baseline resistance at a defined humidity and $R_{25\,\mathrm{RH}}$ the baseline resistance at 25 % RH. It is evident from the data that an increase in the humidity to 50 % RH results in a reduction in the baseline resistance, with the exception of the MPA-stabilized Au NPs, which exhibit a slight increase. Furthermore, an increase in the relative humidity to 75 % results in a slight increase in baseline resistance when compared to the 50 % RH. Notably, citrate Au NPs and PEG–MUA Au NPs demonstrate an elevated baseline resistance at 75 % RH in comparison to their baseline resistance at 25 % RH.

$$\text{normalized resistance change} = \left(\frac{R_{x\,\%\,\mathrm{RH}}}{R_{25\,\%\mathrm{RH}}} \cdot 100\right) - 100\,\% \tag{2}$$

The relative humidity has a significant effect on sensor response of $CO_2$ (Fig. 9) of the various stabilized Au NPs. The pure $CuO/Cu_2O$ (Fig. 9a) does not exhibit a sensor response to $CO_2$ exposure. The citrate (Fig. 9b) shows an increase of the sensor response by an increase in the relative humidity. In the case of citrate Au NPs (Fig. 9c), the sensor response at 25 % RH is the highest across all humidity levels. An increase in humidity to 50 % resulted in a reduction in sensor response, whereas an increase to 75 % RH led to an enhancement in sensor response. However, the concentration dependency is not affected by the different humidity levels. It is demonstrated that the sensor response at concentrations of 1000 and 2000 ppm is comparable across all humidity levels. The sensor is capable of distinguishing between the lower concentrations and 4000 ppm at all humidity levels. The MPA Au NP (Fig. 9d) and PEG–MUA Au NP (Fig. 9e) functionalized sensors demonstrate a reduction in sensor response with an increase in RH. At 75 %, the sensors exhibit no response to $CO_2$ anymore.

Figure 10 illustrates the sensor response towards $HC_{Mix}$ at concentrations of 5, 10, and 20 ppm at varying RH. The pure $CuO/Cu_2O$ (Fig. 10a) exhibits a stable sensor response of approximately 5 % at varying RH. However, the sensor is already saturated at 5 ppm, which precludes the possibility of distinguishing between higher concentrations. The sensor that has been functionalized with citrate demonstrates a slight increase in sensor response to higher humidity lev-

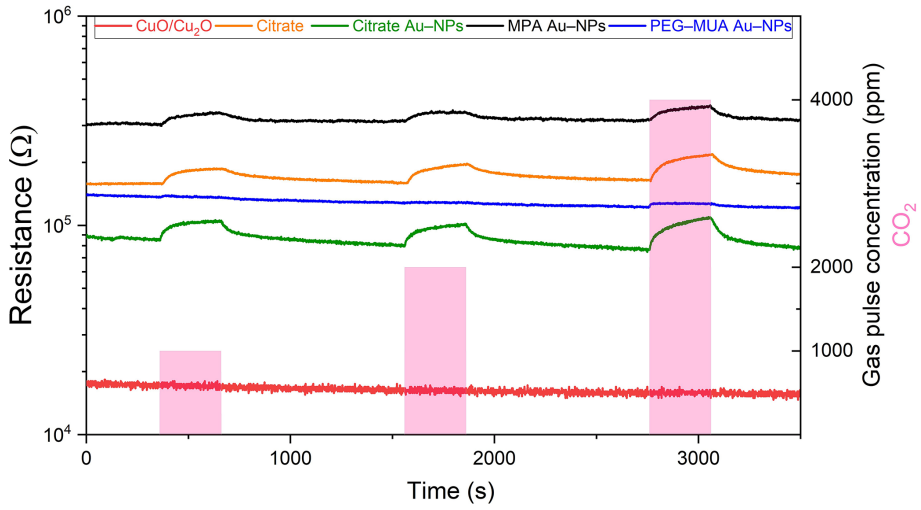


**Figure 6.** Resistance measurement during the exposure of 1000, 2000, and 4000 ppm of $CO_2$ at 300 °C and 50 % RH.

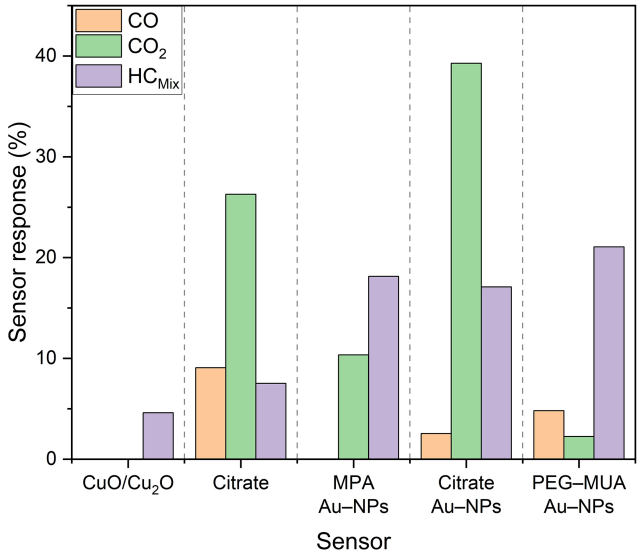


**Figure 7.** Sensor response towards 4000 ppm $CO_2$, 20 ppm CO, and $HC_{Mix}$ at 300 °C and 50 % RH.

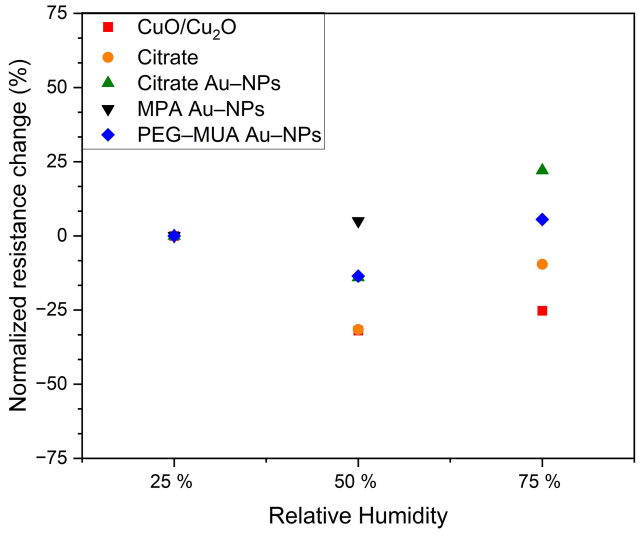


**Figure 8.** Normalized resistance change caused by the change of 25 %, 50 %, and 75 % RH levels.

els. The sensors with citrate-stabilized (Fig. 10c) and PEG–MUA-stabilized (Fig. 10e) Au NPs achieve the highest sensor response at 50 % RH. The sensors also reach saturation at 10 ppm, but it is possible to distinguish between 5 and 10 ppm at all humidity levels. The MPA Au NPs (Fig. 7d) result in a stable sensor response at 50 % and 75 %.

Figure 11 illustrates the sensor response towards CO for concentrations of 5, 10, and 20 ppm at various RH. The sensors comprising pure $CuO/Cu_2O$ (Fig. 11a) and functionalized with MPA-stabilized Au NPs (Fig. 11d) did not exhibit a sensor response to the CO test gas. In the case of citrate (Fig. 11b) and citrate Au NPs (Fig. 11c), the sensor response exhibits a slight increase with rising RH. Conversely, the PEG–MUA Au NPs (Fig. 11e) demonstrate a sensor response of only 4.8 % for 20 ppm at 50 % RH. Notably, the sensor response to CO is particularly weak in comparison to the other test gases.

## 6.5 Temperature dependence

Figure 12 illustrates the measurement of the pure $CuO/Cu_2O$ and functionalized sensors. The pure $CuO/Cu_2O$ (red line) demonstrates no change in resistance during exposure to 4000 ppm $CO_2$. The base resistance is not particularly stable, exhibiting an increase in noise with an increase in temperature. In the case of the MPA (black line) and PEG–MUA (blue line) Au NPs sensors, no change in resistance was ob-

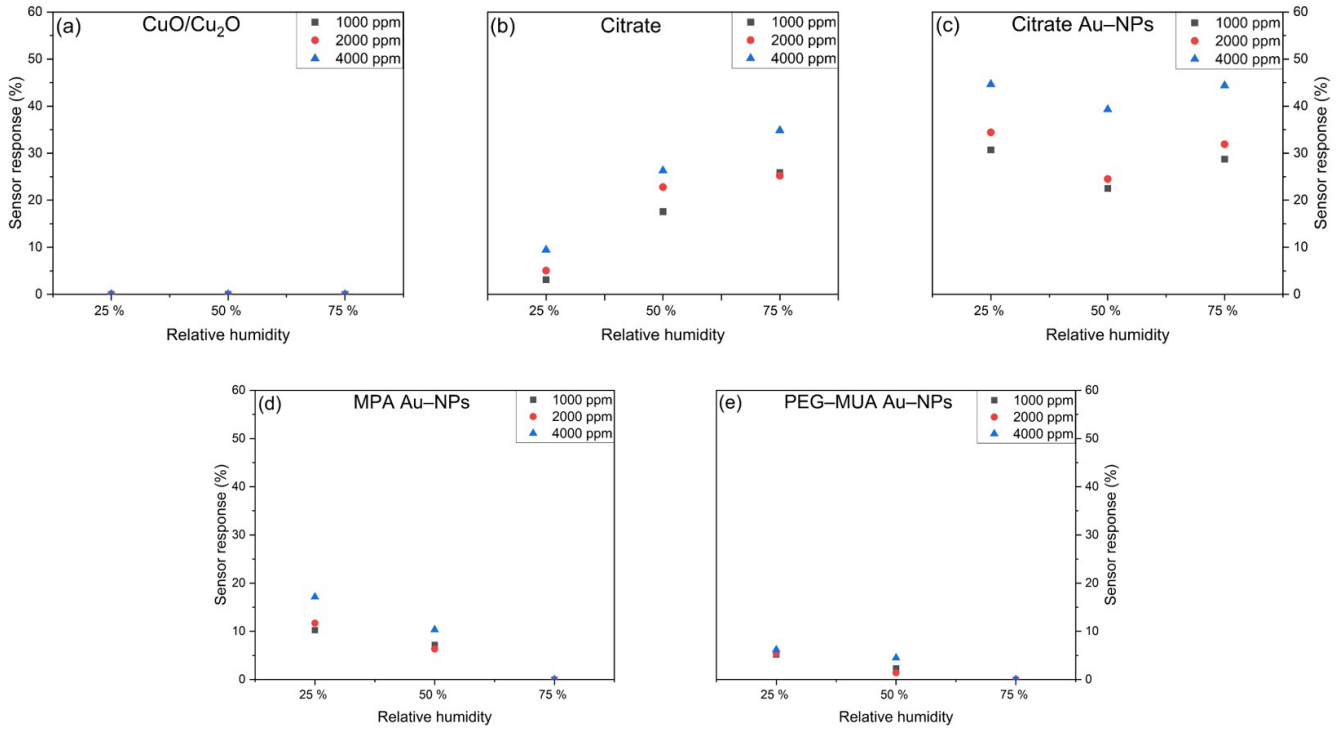


**Figure 9.** Sensor response towards 1000, 2000, and 4000 ppm $CO_2$ at 25 %, 50 %, and 75 % RH of **(a)** bare $CuO/Cu_2O$ and functionalized with **(b)** citrate, **(c)** citrate Au NPs, **(d)** MPA Au NPs, and **(e)** PEG–MUA Au NPs.

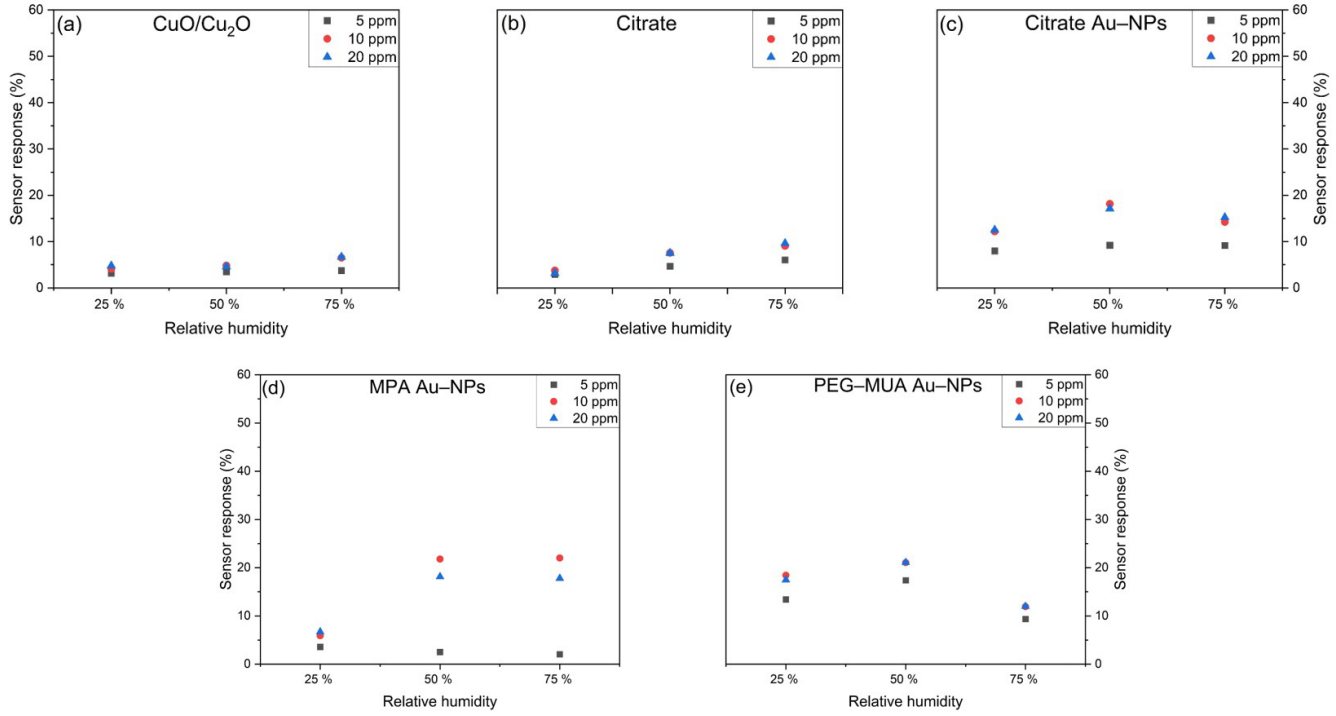


**Figure 10.** Sensor response towards 5, 10, and 20 ppm $HC_{Mix}$ at 25 %, 50 %, and 75 % RH of **(a)** bare $CuO/Cu_2O$ and functionalized with **(b)** citrate, **(c)** citrate Au NPs, **(d)** MPA Au NPs, and **(e)** PEG–MUA Au NPs.

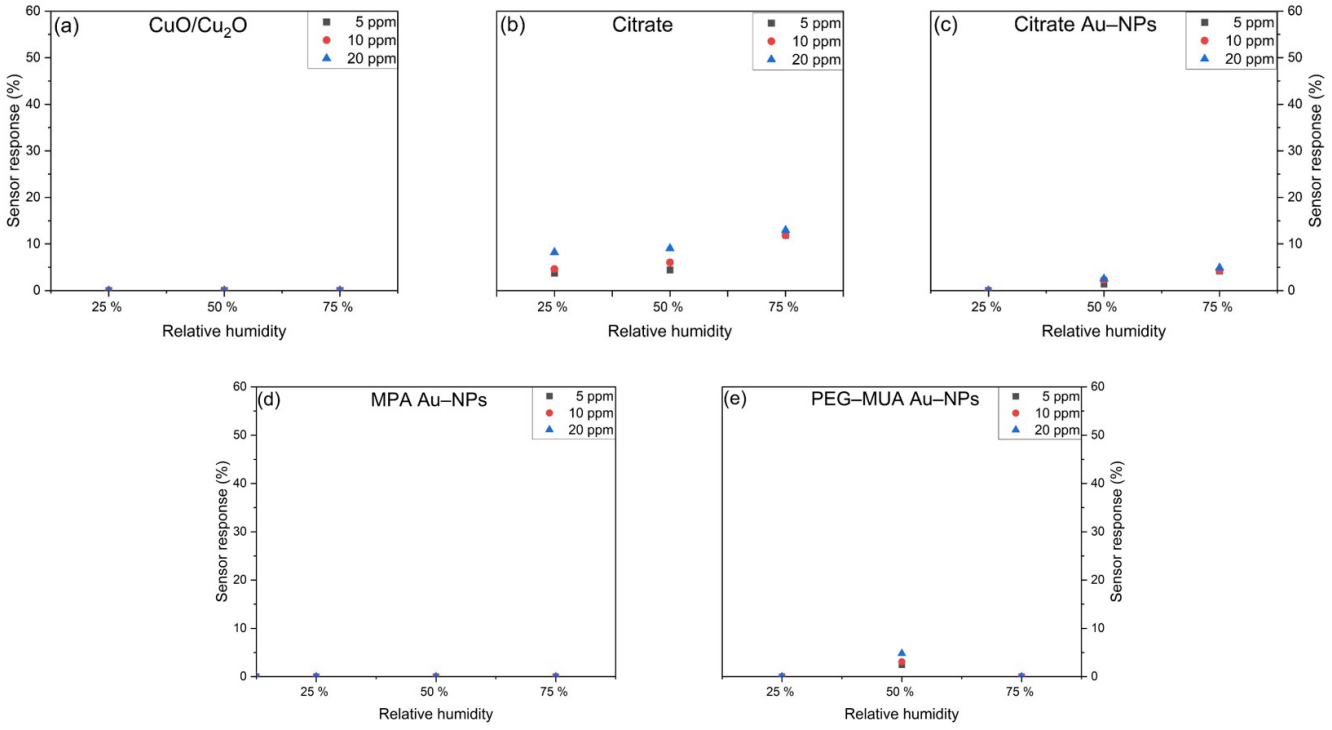


**Figure 11.** Sensor response towards 5, 10, and 20 ppm CO at 25 %, 50 %, and 75 % RH of **(a)** bare $CuO/Cu_2O$ and functionalized with **(b)** citrate, **(c)** citrate Au NPs, **(d)** MPA Au NPs, and **(e)** PEG–MUA Au NPs.

served. However, the base resistance exhibited greater stability across the entire temperature range. The sensor functionalized with citrate (orange line) demonstrates a change in resistance at all temperatures during the exposure period. However, the baseline resistance of citrate-functionalized sensors exhibits a drift at temperatures above 320 °C. Notably, the sensors functionalized with citrate Au NPs also display a change in resistance during the exposure. The baseline is noisy but does not show a drift over the temperature range.

Figure 13 illustrates the sensor response of citrate and citrate Au NP functionalized sensors. It can be observed that the sensor response at higher temperatures is significantly reduced in comparison to the sensor response at 300 °C. Additionally, the sensor response of citrate functionalized sensors exhibits a maximum at 360 °C. Conversely, the sensors with citrate Au NPs demonstrate a decline in sensor response as the operating temperature increases.

## 7 Conclusions and outlook

We fabricated a metal oxide gas sensor based on $CuO/Cu_2O$ for $CO_2$ detection. The $CuO/Cu_2O$ phases and mixtures were checked by GIXRD measurement, and the surface structure was examined by SEM. The gas-sensing performance of the materials towards $CO_2$ was investigated by resistance measurements. Moreover, cross-sensitivity of the sensors was tested against other gases such as CO and $HC_{Mix}$. The type of ligands has an impact on the sensing behaviour of CuO-based sensors. For $HC_{Mix}$, the response is almost the same for all three types of Au NPs, while the citrate-stabilized Au NPs are the best choice for optimizing the $CO_2$ response. The sensor response to $CO_2$ strongly depends on the used ligands; the highest sensor response (39 %) for $CO_2$ is achieved by Au NPs stabilized with citrate. Moreover, the sensors that have been functionalized with citrate without Au NPs demonstrate a good sensor response of 26 % for $CO_2$. The SEM investigation demonstrated that the clustering of Au NPs in the case of citrate Au NPs and MPA Au NPs resulted in an enhanced sensor response towards $CO_2$ compared to the PEG–MUA Au NPs, which exhibited a more uniform distribution over the $CuO/Cu_2O$ surface. In the case of $CO_2$, the sensor can only distinguish between high and low concentrations. A change of the reaction mechanism might explain this observation. The response to CO depends on the ligands as well. Sensors with MPA-stabilized Au NPs show no response to CO. It is imperative to utilize Au NPs in comparison to citrate as Au NPs stabilize the base resistance and also mitigate the impact of humidity.

These differences in behaviour of the functionalized films in dependence of their ligands could be due to different insufficient thermal degradation of the ligands. Organic residuals at 300 °C operations might hamper the interaction of the gas molecules with the Au NPs and the CuO surface. Furthermore, the ligands have an influence on the sensor depen-

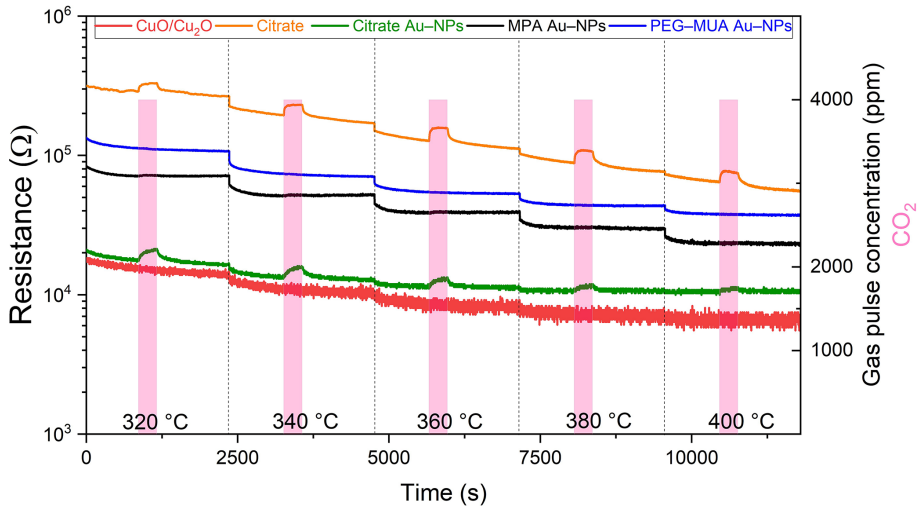


**Figure 12.** Resistance measurement during the exposure of 4000 ppm of $CO_2$ and 50 % RH at an increasing sensor temperature from 320 to 400 °C with 20 °C steps.

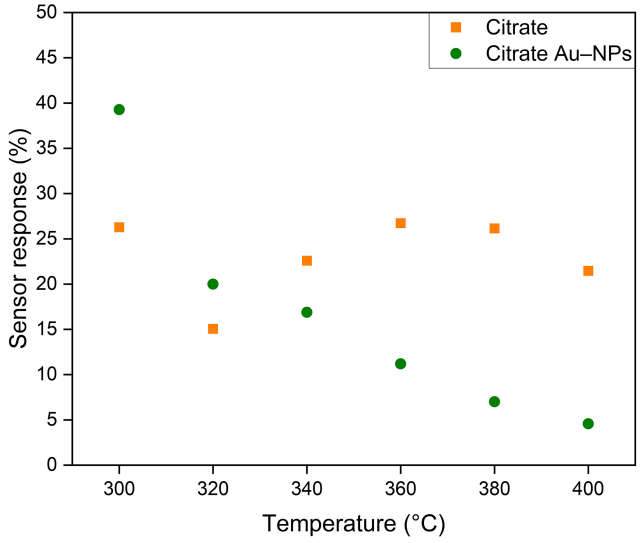


**Figure 13.** Sensor response over the temperature range from 300 to 400 °C for $CuO/Cu_2O$ functionalized with citrate and citrate Au NPs.

dence on humidity for the different test gases. It is possible that the observed phenomena may be attributed to interactions between the organic residuals, specifically the bonding of sulfur groups to the Cu. It is also reported in the literature (Ihs and Liedberg, 1990) that MPA can be easily adsorbed by linking the sulfur group to the surface of Au or Cu. Additionally, the reactions of these organic residuals with the $H_2O$ molecules may also be a contributing factor. Further investigations, e.g. studies of other ligands and NPs, are necessary to reveal the reason for this behaviour.

**Code and data availability.** All the measurement data and codes are not publicly available but can be made available upon request to the corresponding author.

**Author contributions.** CM and LE are responsible for conceptualization; SB and JSN fabricated the nanoparticles; CM fabricated and functionalized the gas sensors; CM and LE performed the gas measurements; CM and KR were responsible for writing (original draft preparation); CM, KR, and AK were responsible for writing (review and editing); AK was responsible for project administration. All authors have read and agreed to the published version of the paper.

**Competing interests.** The contact author has declared that none of the authors has any competing interests.

**Disclaimer.** Publisher's note: Copernicus Publications remains neutral with regard to jurisdictional claims made in the text, published maps, institutional affiliations, or any other geographical representation in this paper. While Copernicus Publications makes every effort to include appropriate place names, the final responsibility lies with the authors.

**Special issue statement.** This article is part of the special issue "Eurosensors 2024". It is a result of the EUROSENSORS XXXVI, Debrecen, Hungary, 1–4 September 2024.

**Acknowledgements.** We gratefully acknowledge Anton Paar GmbH for the loan of the XRDynamic 500 powder diffractometer used in this work and Bernhard Gadermaier from the Institute

for Chemistry and Technology of Materials (ICTM, TU Graz) for carrying out the measurements.

**Financial support.** The authors received financial support under the scope of the COMET programme within the K2 Center "Integrated Computational Material, Process and Product Engineering (IC-MPPE)" conference (grant no. 886385). This programme is supported by the Austrian Federal Ministry for Climate Action, Environment, Energy, Mobility, Innovation and Technology (BMK) and Federal Ministry for Labour and Economy (BMAW), represented by the Austrian Research Promotion Agency (FFG), and the federal states of Styria, Upper Austria, and Tyrol.

**Review statement.** This paper was edited by Gabor Battistig and reviewed by two anonymous referees.

## References

Degler, D., Weimar, U., and Barsan, N.: Current Understanding of the Fundamental Mechanisms of Doped and Loaded Semiconducting Metal-Oxide-Based Gas Sensing Materials, ACS Sensors, 4, 2228–2249, https://doi.org/10.1021/acssensors.9b00975, 2019.

de Los Santos Valladares, L., Salinas, D. H., Dominguez, A. B., Najarro, D. A., Khondaker, S. I., Mitrelias, T., Barnes, C., Aguiar, J. A., and Majima, Y.: Crystallization and electrical resistivity of $Cu_2O$ and CuO obtained by thermal oxidation of Cu thin films on $SiO_2$/Si substrates, Thin Solid Films, 520, 6368–6374, https://doi.org/10.1016/j.tsf.2012.06.043, 2012.

Ihs, A. and Liedberg, B.: Chemisorption of L-Cysteine and 3-Mercaptopropionic Acid on Gold and Copper Surfaces: An Infrared Reflection-Absorption Study, J. Colloid Interf. Sci., 144, 282–292, https://doi.org/10.1016/0021-9797(91)90259-b, 1990.

Jamkhande, P. G., Ghule, N. W., Bamer, A. H., and Kalaskar, M. G.: Metal nanoparticles synthesis: An overview on methods of preparation, advantages and disadvantages, and applications, J. Drug Deliv. Sci. Tec., 53, 101174, https://doi.org/10.1016/j.jddst.2019.101174, 2019.

Kaliyaraj Selva Kumar, A., Zhang, Y., Li, D., and Compton, R. G.: A mini-review: How reliable is the drop casting technique?, Electrochem. Commun., 121, 106867, https://doi.org/10.1016/j.elecom.2020.106867, 2020.

Kaur, J., Khanna, A., Kumar, R., and Chandra, R.: Growth and characterization of $Cu_2O$ and CuO thin films, J. Mater. Sci.-Mater. El., 33, 16154–16166, https://doi.org/10.1007/s10854-022-08506-0, 2022.

Korotcenkov, G., Brinzari, V., and Cho, B. K.: Conductometric gas sensors based on metal oxides modified with gold nanoparticles: a review, Microchim. Acta, 183, 1033–1054, https://doi.org/10.1007/s00604-015-1741-z, 2016.

Maier, C., Egger, L., Köck, A., Becker, S., and S. Niehaus, J.: OT5.154 – Gas Sensing Performance of CuO Sensors Functionalized with Different Stabilized Au-NP, in: Lectures, Debrecen (Hungary), 1–4 September 2024, 119–120, https://doi.org/10.5162/EUROSENSORSXXXVI/OT5.154, 2024a.

Maier, C., Leitgeb, V., Egger, L., and Köck, A.: Size-Dependent Thresholds in CuO Nanowires: Investigation of Growth from Microstructured Thin Films for Gas Sensing, Nanomaterials, 14, 1207, https://doi.org/10.3390/nano14141207, 2024b.

Maier, C., Egger, L., Köck, A., and Reichmann, K.: A Review of Gas Sensors for $CO_2$ Based on Copper Oxides and Their Derivatives, Sensors, 24, 5469, https://doi.org/10.3390/s24175469, 2024c.

Mohamed, S. H. and Al-Mokhtar, K. M.: Characterization of $Cu_2O$/CuO nanowire arrays synthesized by thermal method at various temperatures, Appl. Phys. A-Mater., 124, 493, https://doi.org/10.1007/s00339-018-1914-9, 2018.

Mroczka, R. and Słodkowska, A.: The properties of the polyethylene glycol complex PEG(Na+)(Cu+) on the copper electrodeposited layer by Time-of-Flight Secondary-Ion Mass Spectrometry. The new insights, Electrochim. Acta, 339, 135931, https://doi.org/10.1016/j.electacta.2020.135931, 2020.

Nikolic, M. V., Milovanovic, V., Vasiljevic, Z. Z., and Stamenkovic, Z.: Semiconductor Gas Sensors: Materials, Technology, Design, and Application, Sensors-Basel, 20, 22, https://doi.org/10.3390/s20226694, 2020.

Rydosz, A.: The Use of Copper Oxide Thin Films in Gas-Sensing Applications, Coatings, 8, 425, https://doi.org/10.3390/coatings8120425, 2018.

Schulz, F., Vossmeyer, T., Bastús, N. G., and Weller, H.: Effect of the spacer structure on the stability of gold nanoparticles functionalized with monodentate thiolated poly(ethylene glycol) ligands, Langmuir, 29, 9897–9908, https://doi.org/10.1021/la401956c, 2013.

Schulz, F., Homolka, T., Bastús, N. G., Puntes, V., Weller, H., and Vossmeyer, T.: Little adjustments significantly improve the Turkevich synthesis of gold nanoparticles, Langmuir, 30, 10779–10784, https://doi.org/10.1021/la503209b, 2014.

Steinhauer, S.: Gas Sensors Based on Copper Oxide Nanomaterials: A Review, Chemosensors, 9, 51, https://doi.org/10.3390/chemosensors9030051, 2021.

Su, Y.-T., Lan, G.-Y., Chen, W.-Y., and Chang, H.-T.: Detection of copper ions through recovery of the fluorescence of DNA-templated copper/silver nanoclusters in the presence of mercaptopropionic acid, Anal. Chem., 82, 8566–8572, https://doi.org/10.1021/ac101659d, 2010.

Tehrani, F. S.: Transformation from amorphous to nanocrystalline SiC thin films prepared by HWCVD technique without hydrogen dilution, B. Mater. Sci., 38, 1333–1338, https://doi.org/10.1007/s12034-015-1018-5, 2015.

Thambiliyagodage, C.: Ligand exchange reactions and PEG stabilization of gold nanoparticles, Current Research in Green and Sustainable Chemistry, 5, 100245, https://doi.org/10.1016/j.crgsc.2021.100245, 2022.

Velmathi, G., Mohan, S., and Henry, R.: Analysis of Factors for Improving Functionality of Tin Oxide Gas Sensor, IETE Tech. Rev., 33, 122–129, https://doi.org/10.1080/02564602.2015.1049224, 2016.

Wang, Y. Q., Liang, W. S., and Geng, C. Y.: Shape evolution of gold nanoparticles, J. Nanopart. Res., 12, 655–661, https://doi.org/10.1007/s11051-009-9612-3, 2010.

Wimmer-Teubenbacher, R., Sosada-Ludwikowska, F., Travieso, B., Defregger, S., Tokmak, O., Niehaus, J., Deluca, M., and Köck, A.: CuO Thin Films Functionalized with Gold Nanoparticles for

Conductometric Carbon Dioxide Gas Sensing, Chemosensors, 6, 56, https://doi.org/10.3390/chemosensors6040056, 2018.

Xiong, L., Xiao, H., Chen, S., Chen, Z., Yi, X., Wen, S., Zheng, G., Ding, Y., and Yu, H.: Fast and simplified synthesis of cuprous oxide nanoparticles: annealing studies and photocatalytic activity, RSC Adv., 4, 62115–62122, https://doi.org/10.1039/C4RA12406E, 2014.

Yang, Y., Yang, L., and Feng, S.: Interfacial engineering and film-forming mechanism of perovskite films revealed by synchrotron-based GIXRD at SSRF for high-performance solar cells, Materials Today Advances, 6, 100068, https://doi.org/10.1016/j.mtadv.2020.100068, 2020.